BNL--32262

DE83 003944

Conf-821011--22

BNL 32262

OG 663

Contributed Paper at the
1982 Nuclear Science Symposium
Washington, D.C. Oct. 20-22, 1982

Study of the Electric Field Inside Microchannel Plate Multipliers

F. Gatti[a], K. Oba[b] and P. Rehak

Brookhaven National Laboratory, Upton, NY 11973

a) Permanent address: Istituto di Fisica Politecnico, Milano, Italy.
b) Permanent address: Hamamatsu TV Co., Ltd., Hamamatsu, Japan

Study of the Electric Field Inside Microchannel Plate Multipliers[a)]

E. Gatti[b)], K. Oba[c)] and P. Rehak
Brookhaven National Laboratory
Upton, New York 11973

Abstract

Electric field inside high gain microchannel plate multipliers was studied. The calculations were based directly on the solution of the Maxwell equations applied to the microchannel plate (MCP) rather than on the conventional lumped RC model. The results are important to explain the performance of MCP's, i) under a pulsed bias tension and, ii) at high rate conditions. The results were tested experimentally and a new method of MCP operation free from the positive ion feedback was demonstrated.

I. Introduction

This paper investigates the electric field inside microchannel plate multipliers (MCP) i) under pulsed applied tension and ii) due to electrons participating in a cascade and leaving the channel of an MCP.

The analysis is performed for a standard MCP with the conductivity due to the surface of the channel walls only and for a hypothetical MCP having a certain bulk conductivity.

Section II of the paper studies the behavior of an MCP under pulsed applied tension theoretically and experimentally. A new method of MCP operation free from positive ion feedback is shown.

Section III studies the change of the electric field inside an MCP due to the multiplication process itself. It is shown that the channel recharging time of a standard MCP is much larger than could be guessed by a naive RC model. The possible improvement due to the bulk conductivity of a hypothetical MCP is shown.

II. MCP Under Pulsed Applied Tension

A. Theory

Figure 1 shows an MCP with the bias cut angle α defined as an angle between the axis of the channel and the normal to the face plane of an MCP.

First, let us consider a steady (DC) tension applied between the input and the output face of an MCP. One channel of a biased MCP together with its conductive surface unfolded and placed into the x-y plane is also shown in Fig. 1. The channel surface was cut in a plane containing the channel axis and a normal to the MCP face, (design plane on the left side of the Fig. 1) thus the upper and lower boundaries of the unfolded surface have the form of the simple cosine function.

Under steady conditions the potential U on the unfolded surface in the x-y plane has to obey Laplace's equation

$$\Delta U = 0 \qquad (1)$$

The potentials of the upper and lower boundaries are defined by the applied tension.

$$U = 0 \text{ at } y = -r.\mathrm{tg}\alpha.\cos(x/r)$$

$$U = U_o \text{ at } y = L - r.\mathrm{tg}\alpha.\cos(x/r) \qquad (2)$$

where r and L are the channel radius and length, respectively, and the bias angle α was defined previously. The vertical boundaries are artificial and the function U has to be periodic with the space period $2\pi r$.

Equation (1) with the given boundary conditions (2) can be solved by the Fourier method of separation. The solution can be written approximately as

$$U(x,y) = \frac{U_o}{L}.y + \frac{U_o}{L}.\mathrm{tg}\alpha.r.\cos(x/r)\frac{\exp(y/r)-\exp(-y/r)}{\exp(L/r)+1}$$

which for $y \ll L$ gives

$$U(x,y) = \frac{U_o}{L}.y + \frac{U_o}{L}.\mathrm{tg}\alpha.r.\cos(x/r).\exp(-y/r) \qquad (3)$$

Equipotentials calculated from equation (3) for the lower part of the x-y plane are shown in Fig. 2. From equation (3) and/or from Fig. 2 we can see that inside an MCP channel (i.e. more than two channel radii from either face of an MCP) the potential is independent of the azimuthal coordinate. Folding the x-y plane back into real space the equipotentials form closed circles perpendicular to the channel axis. Therefore, under steady conditions the electric field in an MCP is parallel to the channel axis.

Secondly, let us consider the electric field after a step tension is applied to the input face of a biased MCP. The electric field at time $t = 0^+$ is similar to the field of a parallel plate capacitor which is perpendicular to the faces of the MCP. Due to the difference of the dielectric constants of the lead glass channel wall and of the vacuum inside the channel the equipotentials are broken at these boundaries. Fig. 3a shows an equipotential line at time $t = 0^+$ which satisfies the well known boundary conditions between the two dielectrics. We can see that the field vector E_o is inclined even more with respect to the channel axis than the field of a simple parallel plate capacitor.

Fig. 3a shows also an equipotential line in the DC limit. When a step tension is applied to the input face the field inside a channel of an MCP is established at the angle θ_{max} relative to the channel

a) This research supported by the U.S. Dept. of Energy under Contract DE-AC02-76CH00016.
b) Permanent address: Istituto di Fisica Politecnico, Milano, Italy.
c) Permanent address: Hamamatsu TV Co., Ltd., Hamamatsu, Japan.

axis and rotates to its steady (DC) direction which coincides with the axis.

The rotation of the electric field is due to the flow of azimuthal currents in the surface of an MCP channel. Fig. 3b shows the other view of an MCP (parallel to the input face) where the azimuthal currents are visible. A negative charge flows towards points A and B from the left hand side and positive charge from the right hand side. Points A and B thus receive zero net charge and represent a virtual ground. For similar symmetry reasons the potential on the lines having the same distance from two neighboring channels (solid hexagon on Fig. 3b) does not change in value and these lines are also considered as ground lines.

The time constant of the rotation of the electric field is thus the time constant of the distributed RC line between points A and B. The resistance per unit length R is related to the total MCP resistance and the capacitance per unit length C is given by the geometry and by the dielectric constant of the channel walls.

The time constant of the fundamental harmonics of a distributed RC line is

$$\tau = \frac{RC\ell^2}{\pi^2} \qquad (4)$$

where ℓ is the length of the line and R,C were previously defined. Expressing the variables in eq.(4) by directly measurable MCP parameters and after simple manipulations we obtain

$$\tau = \left(R_{MCP} \cdot C_{MCP}\right) \frac{2xOAR}{1-OAR} \cdot \frac{D}{D_{cc}-D} \qquad (5)$$

where R_{MCP}, C_{MCP} are the resistance and capacitance of the MCP measured between the input and the output faces, OAR is the open area ratios

$$= \frac{\pi}{2\sqrt{3}} \left(\frac{D}{D_{cc}}\right)^2$$

and D, D_{cc} are the channel diameter and the distance between the axis of two neighboring channels (see Fig. 3b).

The product $R_{MCP} \cdot C_{MCP}$ is the "natural" time constant of the MCP. We see that the electric field rotates at a much slower rate (≈10 times) than that which would correspond to this "natural" time constant.

The direction of the electric field inside an MCP channel influences the electron acceleration along the channel and thus the cascade process[2], and of more importance the positive ion feedback mechanism. This feedback limits the attainable gain of standard straight channel MCPs.

B. Experimental Results

A train of square high tension pulses was applied to the input face of a 2 mm thick Hamamatsu MCP (D = 12.5 μ, D_{cc} = 15μ, OAR = .63, ℓ/D = 160).

The schematics of the high tension pulser and the waveform of the applied high tension are shown in Fig. 4. The switching elements were LED controlled triacs (MOC3021). The relevant time constants were adjusted in such a way that the rise time was 3 μs and the applied tension was constant within ± .1% from 6μs on.

If the time between two consecutive pulses T(Fig. 4b) is much smaller than the time constant of the rotation of the electric field, the angle θ between the direction of the electric field (during the time ΔT when the high tension is applied) and the channel axis is independent of the time constant and given by the following equation

$$\theta = \theta_{max} \cdot \frac{T-\Delta T}{T} \; ; \; T \ll \tau \qquad (6)$$

where θ_{max} is the maximum angle (Fig. 3a).

Amplification characteristics of the MCP as a function of the angle θ were studied. Fig. 5 shows single photoelectron spectra of the MCP excited by a UV-light for different values of the angle θ. A 6 kGauss external (static) magnetic field perpendicular to the MCP faces was applied in order to suppress afterpulses. All spectra show a clear peak; however, the high charge tail which dominates the shape of the distributions is a strong function the angle θ. Fig. 6 summarizes the spectra. It shows the peak gain (the most probable gain) as a function of the angle θ.

The dependence shown in Fig. 6 was used as a calibration for the measurement of the electric field rotation time constant. For this measurement the period T of the pulsed tension (Fig. 4b) was made much longer than the expected time constant. Thus each pulse ΔT can be considered to be an independent step function and the angle θ should change in time according to the simple equation

$$\theta = \theta_{max} \cdot \exp(-t/\tau) \qquad (7)$$

where time t is measured from the leading edge of the high tension pulse. From measured spectra for different time intervals (t,t+Δt) it is possible (making use of the "calibration" in Fig. 6) to deduce the angle θ within this time interval. The result is shown in Fig. 7. The angle between the direction of the electric field and the channel axis θ follows approximately equation (7) with the time constant τ = (230 ± 20)ms. The measured MCP had the "natural" time constant $\tau_{MCP} = R_{MCP} \times C_{MCP}$ = 20 ms, thus the measured value of τ agrees with the equation (5).

The most important result is presented in Fig. 8. It shows the probability of an afterpulse as a function of angle θ. There was no magnetic field in the MCP during this measurement. We can see that already at a small angle between the direction of the electric field and the channel axis the probability of

an afterpulse is substantially reduced, and for more than a half of all possible angles this probability is reduced by two orders of magnitude.

This improvement in the performance of a MCP amplifier can be easily understood. When the direction of the electric field in a MCP channel is inclined with respect to the channel axis positive ions produced by bombarding electrons in the cascade travel a smaller distance backward inside the channel before hitting the channel wall. Thus they have less energy to produce a secondary electron by the impact and restart a new cascade. Moreover the cascade would start closer to the output face of a MCP and thus less likely to develop.

For a large class of applications (gating, strobing, detection around pulsed accelerators, etc.) the MCP is or can be used in a pulsed mode. If the MCP parameters are suitably chosen the time constant of the electric field rotation (equation 5) can be matched with the duty cycle required by the particular application. The operation of the MCP can be practically free of positive ion feedback and a gain up to 10^6 can be obtained from a single straight MCP.

There is a different way to obtain an inclined electric field inside channels of an MCP.[1] If glass walls between channels of an MCP were made from a conductive material the DC-limit equipotential line (upper line in Fig. 3a) in the conductive wall would have to be almost perpendicular to the wall boundaries. Therefore, the electric field in an MCP having conductive walls should always be inclined with respect to the channel axis and the amplification should be practically free from positive ion feedback. In the following section it is shown that such an MCP should also have a better rate performance than a standard channel surface conductive MCP.

III. Rate Limitations of an MCP.

The electric field along a channel of an MCP supplies the energy to the electron cascade process. The field is changed in the process due to the charge of electrons leaving the walls of the channel. The change in the electric field is such that the new field is less suitable to produce a cascade process. The rate capbility of an MCP is related to the time needed to reestablish the electric field along the channel (recharging time constant).

To calculate this recharging time constant, up to now only a crude RC model was used.[3] In our model we treat an MCP as an anisotropic medium where the conductivity and the dielectric constant depend on the direction. To simplify the calculation the cut bias of the MCP angle is supposed to be zero and we close the channel direction along the z-axis. Due to the linearity of the laws of electrodynamics the MCP recharging time in our model is the relaxation time of the anisotropic medium (placed between two grounded parallel conductive plates) after a point charge Q_0 is put into the medium.

Ohm's law for our MCP model is written as:

$$j_x = \sigma_r E_x \; ; \; j_y = \sigma_r E_y \; ; \; j_z = \sigma_z E_z \qquad (8)$$

where j_x, j_y, j_z (x,y,z,t) are the components of the current density; σ_z the mean conductivity along the channel (z) axis; $\sigma_r (=\sigma_x=\sigma_y)$ is the conductivity perpendicular to the channel direction, and E_x, E_y, $E_z(x,y,z,t)$ are the components of the electric field. Gauss' law under the same anisotropic assumptions is written as

$$\varepsilon_r\left(\frac{\partial Ex}{\partial x} + \frac{\partial Ey}{\partial y}\right) + \varepsilon_z \frac{\partial Ez}{\partial z} = \rho \qquad (9)$$

where ε_r, ε_z are the dielectric constants in their respective directions and $\rho(x,y,z,t)$ is the charge density.

The continuity equation has its usual form

$$\operatorname{div} \vec{j} + \frac{\partial \rho}{\partial t} = 0 \qquad (10)$$

We define the electric potential $U(x,y,z,t)$ in a standard way

$$\vec{E} = -\overrightarrow{\operatorname{grad}}\, U \qquad (11)$$

If the output face of the MCP is placed in the plane $z = 0$ and the input face is in the plane $z = \ell$ the boundary conditions are

$$U(x,y,z=0,t) = U(x,y,z=\ell,t) = 0 \qquad (12)$$

Equations (8-12) define mathematically the problem. To find the solution we substitute the current densities j-s from equations (8) into equation 10. We express the electric field $\vec{E}$ using the potential U (equation 11) and take the Laplace transform with respect to time variable t. Equations (9) and (10) can be then written

$$-\varepsilon_r\left(\frac{\partial^2 u}{\partial x^2} + \frac{\partial^2 u}{\partial y^2}\right) - \varepsilon_z \frac{\partial^2 u}{\partial z^2} = \bar{\rho} \qquad (9')$$

$$-\sigma_r\left(\frac{\partial^2 u}{\partial x^2} + \frac{\partial^2 u}{\partial y^2}\right) - \sigma \frac{\partial^2 u}{\partial z^2} + s\bar{\rho} - \rho(x,y,z,t=0) \qquad (10')$$

where $u(x,y,z,s)$, $\bar{\rho}(x,y,z,s)$ are the Laplace transforms of U and ρ, respectively, and s is the Laplace variable. Initial distribution of the charge density in our case is a spatial Dirac's delta function

$$\rho(x,y,z,t=0) = Q_o\, \delta(x-x_o)\,\delta(y-y_o)\,\delta(z-z_o) \qquad (13)$$

where Q_o was defined previously and x_o, y_o, z_o

are the coordinates of the point charge. From equations (9') and (10') we can eliminate ρ and after a rearrangement we obtain

$$(\sigma_r+\varepsilon_r s)\left(\frac{\partial^2 u}{\partial x^2}+\frac{\partial^2 u}{\partial y^2}\right)+(\sigma_z+\varepsilon_z s)\frac{\partial^2 u}{\partial z^2} = -Q_o\delta(x-x_o)\,\delta(y-y_o)\delta(z-z_o). \tag{14}$$

Equation (14) is very similar to "classical" equation of electrostatics

$$\Delta u = -\delta(\vec{r}-\vec{r}_o) \tag{15}$$

with the well known solution

$$u = \frac{1}{4\pi\left|\vec{r}-\vec{r}_o\right|} .$$

The left hand side of the equation (14) can take the form of a simple Laplacian in the new coordinates ξ,η and ζ defined by the following equations.

$$x = \xi\cdot\sqrt{\sigma_r+\varepsilon_r s}$$
$$y = \eta\cdot\sqrt{\sigma_r+\varepsilon_r s} \tag{16}$$
$$z = \zeta\cdot\sqrt{\sigma_z+\varepsilon_z s}$$

Equation (14) thus becomes

$$\frac{\partial^2 u}{\partial\xi^2}+\frac{\partial^2 u}{\partial\eta^2}+\frac{\partial^2 u}{\partial\zeta^2} = -Q_o\frac{\delta(\xi-\xi_o)\delta(\eta-\eta_o)\delta(\zeta-\zeta_o)}{(\sigma_r+\varepsilon_r s)\sqrt{\sigma_z+\varepsilon_z s}} \tag{17}$$

where in the right hand side of equation (17) we have used the formal relation

$$\delta[(k(\xi-\xi)] = \frac{1}{k}\ \delta(\xi-\xi_o) \tag{18}$$

where k is an arbitrary constant. Equation (17) is no identical to equation (15) which allows us to write down immediately the solution.

$$u(\xi,\eta,\zeta,s) = \frac{Q_o}{4\pi(\sigma_r+\varepsilon_r s)\sqrt{\sigma_z+\varepsilon_z s}}\cdot \frac{1}{\sqrt{(\xi-\xi_o)^2+(\eta-\eta_o)^2+(\zeta-\zeta_o)^2}} \tag{19}$$

Now we can return to the space coordinate x,y,z and from equation (19), after some cumbersome algebra, obtain the following expression

$$u(x,y,z,s) = \frac{Q_o}{4\pi\varepsilon_r\sqrt{\gamma(r-r_o)^2+(z-z_o)^2}}\ \frac{1}{\sqrt{1/\tau_r+s}}\ \frac{1}{\sqrt{b+s}} \tag{20}$$

where $\gamma = \varepsilon_z/\varepsilon_r$; $\tau_r = \varepsilon_r/\sigma_r$; $\tau_z = \varepsilon_z/\sigma_z$;

$$(r-r_o)^2 = (x-x_o)^2+(y-y_o)^2$$

and $$b = \frac{\gamma(r-r_o)^2/\tau_z+(z-z_o)^2/\tau_r}{\gamma(r-r_o)^2+(z-z_o)^2} .$$

The form of equation (20) has a known Laplace inverse-transform which is:

$$U(x,y,z,t) = \frac{Q_o}{4\pi E_r\sqrt{\gamma(r-r_o)^2+(z-z_o)^2}}\cdot\exp\left[-\tfrac{1}{2}(b+1/\tau_r)t\right] \cdot I_o\left(\tfrac{1}{2}(b-1/\tau_r)t\right) . \tag{21}$$

where I_o is the Modified Bessel Function. Equation (21) is a solution of differential equations (9) and (10) but it does not satisfy the boundary conditions (12). The final solution of our problem is an infinite sum of terms (21) where source positions are reflected in conductive planes z = 0 and Z = ℓ. (Standard method of reflections.)

In the special case of an isotropic medium ($\varepsilon_r=\varepsilon_z=\varepsilon_i$, $\sigma_r = \sigma_z$) equation (21) reduces into

$$U(x,y,s,t) = \frac{Q_o}{4\pi\varepsilon_i\sqrt{r^2-r_o)^2+(z-z_o)^2}}\cdot\exp(-t/\tau_i) \tag{22}$$

where $\tau_i(=\tau_r=\tau_z) = R_{MCP}\cdot C_{MCP}$ is the "natural" time constant of an MCP.

Recharging behavior of different MCP's was studied by evaluating the sum of solutions (21). Fig. 9a shows the time development of the voltage along a channel of a 1 mm thick standard MCP with the conductivity exclusively due to the channel surface. (σ_r=0, one directional conductivity.) The charge

Q_o (= .1pC) was put .2 mm from the output face of an MCP imitating the effect of electrons belonging to a cascade and leaving the channel. The voltage is shown for a channel with a cascade in it and for its first and second neighbor (total 1,6 and 12 channels for a close packed hexagonal structure of a MCP.) Ten individual curves are spaced by increments of half the "natural" time constant from 0 (the cascade time) to 5 τ_z. We can see that the decay is slow and after a lapsed time of 5 τ_z the voltage is still about 40% of the initial perturbation.

Fig. 9b shows the same results for a hypothetical MCP with an isotropic conductivity. According to equation (22) the initial perturbance decays exponentially with the "natural" time constant of the MCP. We can see that after a time 5τ the remaining voltage is at .5% the level of the initial value.

The isotropic conductivity of an MCP is impossible to realize. Fig. 9c shows the relaxation properties of a hypothetical MCP made of conductive glass wall where the average $\sigma_r = \sigma_z/2$. The decay of the initial perturbance is slower than for an isotropic MCP; however, it is substantially faster than for a standard linear conductive MCP.

The reason for the shorter decay time of bulk conductive MCPs is the presence of the radial current contributing to the neutralization of the charge Q_o. The absence of these radial currents in the case of a standard MCP requires all the charge to be supplied along one channel with its full resistance resulting in a longer decay time.

Comparing Fig. 9a,b,c we can conclude that the bulk conductivity MCP improves substantially the rate capability of an MCP when compared with a standard MCP of the same DC power dissipation.

Conclusions

It was shown that i) a standard MCP can be operated practically free from positive ion feedback under a pulsed applied tension at the sacrifice of the duty cycle. A hypothetical bulk conductive MCP should operate free of feedback under any DC applied tension.

ii) the rate capability of an MCP could also be substantially increased by the effect of the bulk conductivity.

We would like to thank R. Boie now at Bell Telephone Laboratories for the design of the high tension pulser.

References

1. We are indebted to Dr. C. Tosswill from Galileo for bringing our attention to this fact.
2. K. Oba and H. Maeda, An Analysis of the Direct Current Operation of Channel Electron Multipliers, Advances in Electronics and Electron Physics, Vol. 33A, 183 (1972).
3. E.H. Eberhardt, An Operational Model for Microchannel Plate Devices, IEEE Transactions on Nuclear Science, NS-28, 712 (1981).

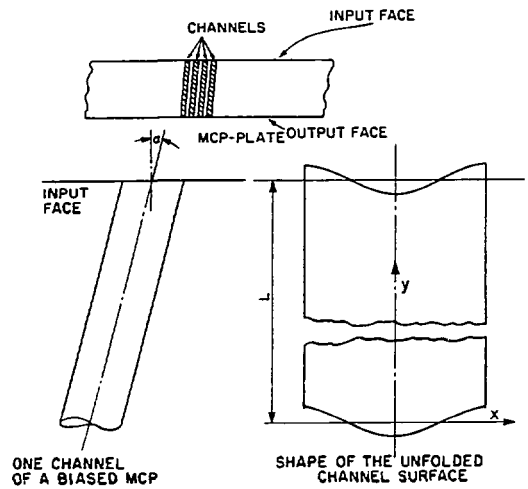

Fig. 1. MCP with a bias cut angle α. The surface of a channel shown at the left hand side was cut in the paper plane and unfolded.

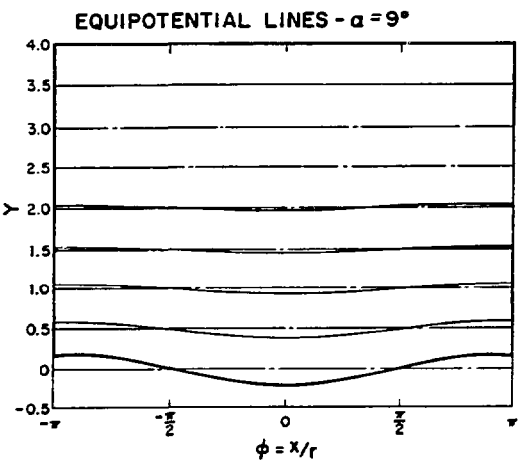

Fig. 2. Equipotential lines in a DC limit of the unfolded channel surface. The thick line shows the lower boundary of the channel surface.

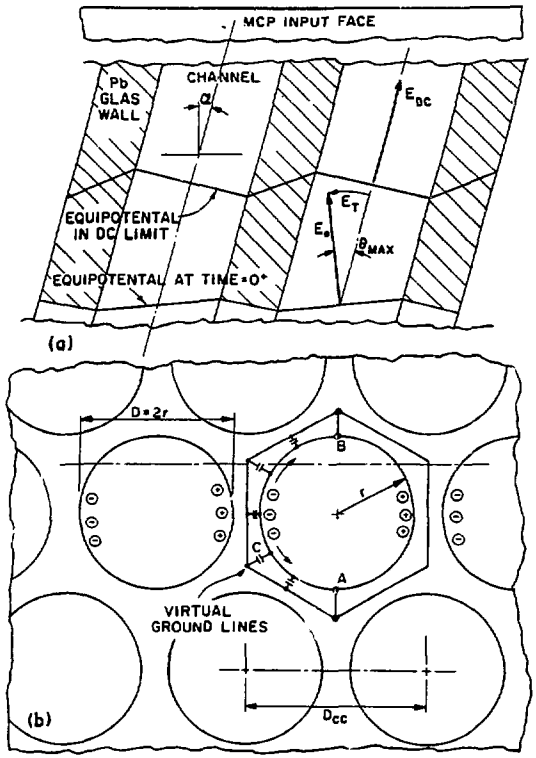

Fig. 3. a) Equipotential lines and electric field vectors inside a standard MCP. α is the bias cut angle, θ_{max} is the maximum angle between the direction of the electric field and the channel axis. The lower line showing the configuration of the field at time $t = 0^+$ for the pulsed applied tension is similar to a steady field of a bulk conductive MCP. b) Azimuthal currents responsible for the field rotation in an MCP. C is the distributed capacitance between the conductive channel surface and the virtual ground.

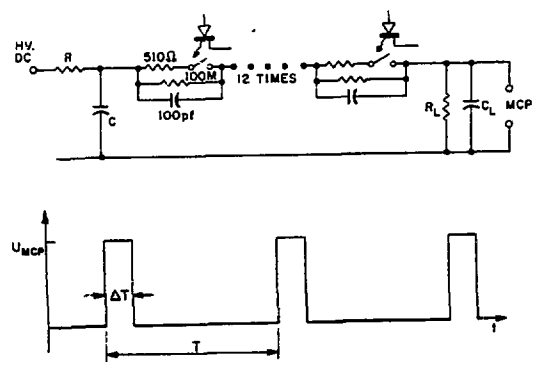

Fig. 4. a) Schematic of the pulser of the applied tension. b) The applied waveform.

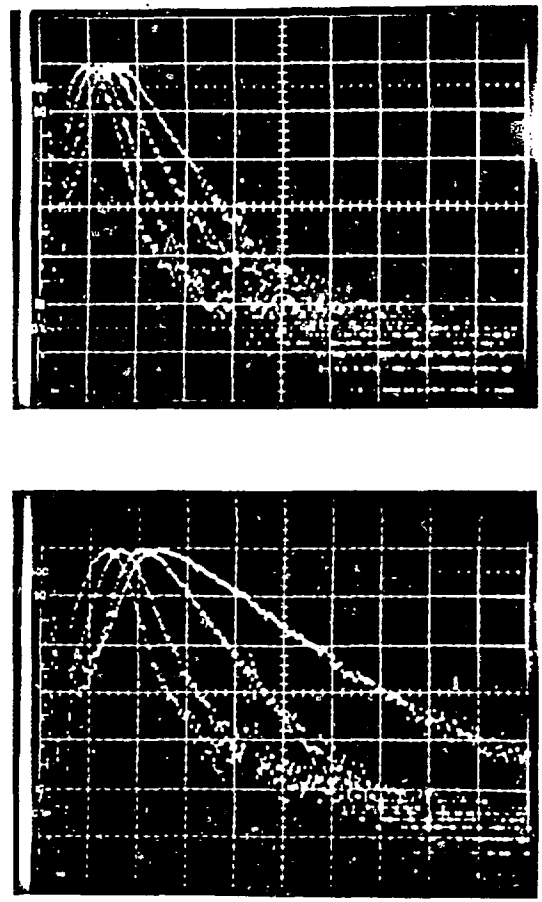

Fig. 5. Single photoelectron spectra for different angles between the electric field and the channel axis in a magnetic field. The vertical scale showing the number of events is logarithmic where 2 divisions equal a factor 10. On the horizontal scale one division corresponds to the gains of 4×10^5.

a) spectra for θ = 17,15,13 and 11°.

b) spectra for θ = 15°,13°,9° and 5° (the peak positon moves to the right with decreasing angle).

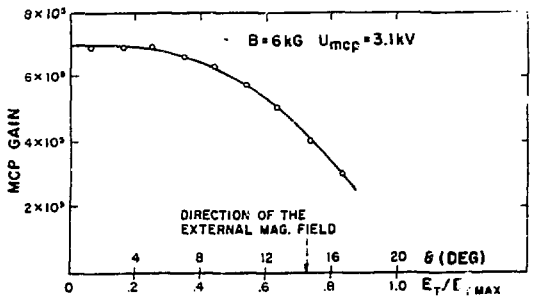

Fig. 6. The most probable gain (peak position) as a function of the angle between the electric field and the channel axis.

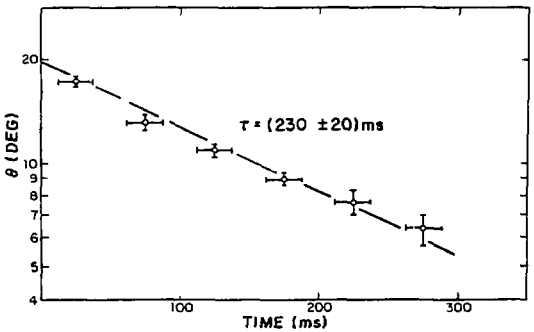

Fig. 7. The angle θ between the electric field and the channel axis as a function of time from the leading edge of the applied pulse.

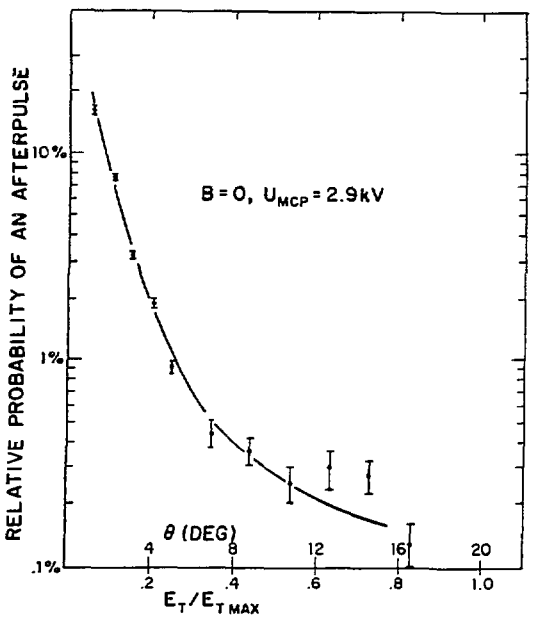

Fig. 8. Relative probability of an afterpulse for the MCP with no magnetic field as a function of angle θ. For angles larger than 8° we can see practically no positive ion feedback.

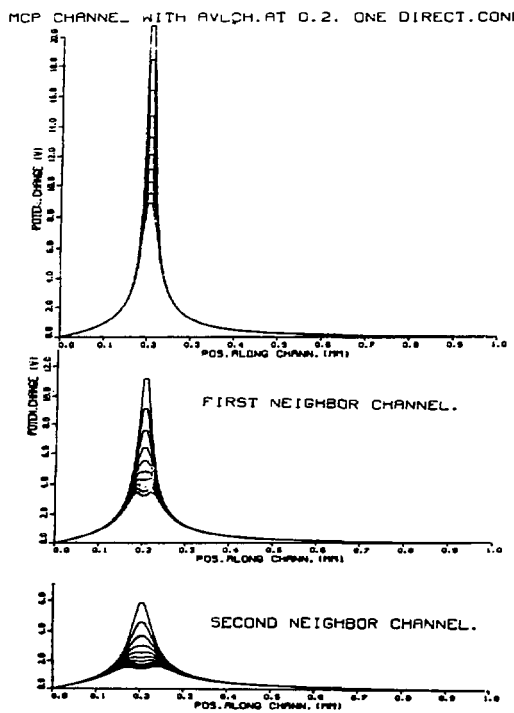

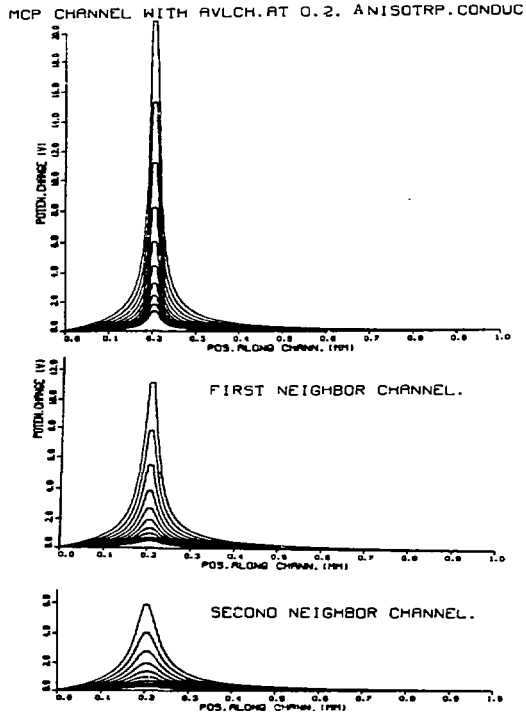

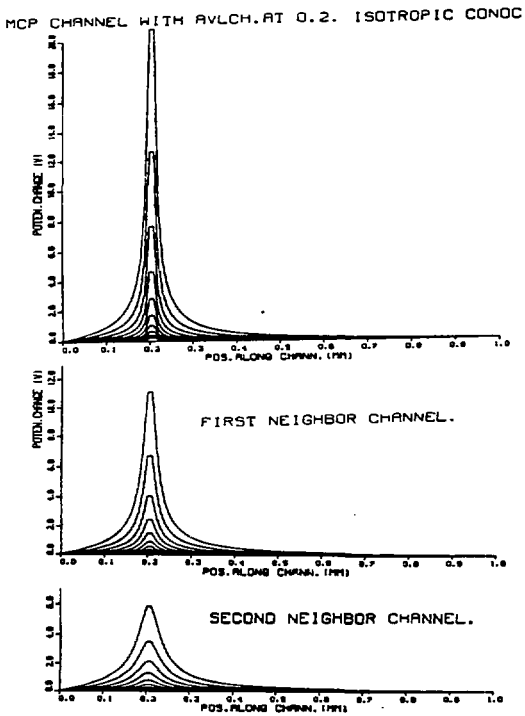

Fig. 9. Development of the voltage along channels of a 1 mm thick MCP. A point charge of .1pC was deposited .2 mm from the output face. The voltage is shown along the channel where the charge was deposited as well as for the first and the second neighbor channel. Individual curves are spaced $\Delta t = \tau_z/1$ in time ($\tau_z = R_{MCP} \times C_{MCP}$) starting at time = 0 up to 5 τ_z. a) for a standard MCP with the conductivity exclusively due to the channel surfaces. b) for a hypothetical MCP with isotropic conductivity. c) for a hypothetical MCP with $\sigma_r = \sigma_z/2$.